



HAL
open science

Reactivity of secondary phases in weathered limestone using isotopic tracers (D and ^{18}O): the case study of the 'Tribunal Administratif' of Paris

Lucile Gentaz, Mandana Saheb, Aurélie Verney-Carron, Loryelle Sessegolo, Anne Chabas, Nicolas Nuns, Laurent Remusat, Adriana Gonzalez-Cano, Chloé Fourdrin, Jean-Didier Mertz, et al.

► To cite this version:

Lucile Gentaz, Mandana Saheb, Aurélie Verney-Carron, Loryelle Sessegolo, Anne Chabas, et al.. Reactivity of secondary phases in weathered limestone using isotopic tracers (D and ^{18}O): the case study of the 'Tribunal Administratif' of Paris. *Environmental Science and Pollution Research*, 2020, 28 (3), pp.2810-2821. 10.1007/s11356-020-10644-z . hal-03402473

HAL Id: hal-03402473

<https://hal.science/hal-03402473v1>

Submitted on 25 Oct 2021

HAL is a multi-disciplinary open access archive for the deposit and dissemination of scientific research documents, whether they are published or not. The documents may come from teaching and research institutions in France or abroad, or from public or private research centers.

L'archive ouverte pluridisciplinaire **HAL**, est destinée au dépôt et à la diffusion de documents scientifiques de niveau recherche, publiés ou non, émanant des établissements d'enseignement et de recherche français ou étrangers, des laboratoires publics ou privés.

Manuscript Number: STOTEN-D-20-08334

Title: Reactivity of secondary phases in weathered limestone using isotopic tracers (D and 18O): the case study of the 'Tribunal Administratif' of Paris

Article Type: Research Paper

Keywords: limestone, weathering, air pollution, syngenite, secondary phase

Corresponding Author: Dr. Aurélie Verney-Carron,

Corresponding Author's Institution:

First Author: Lucile Gentaz

Order of Authors: Lucile Gentaz; Mandana Saheb; Aurélie Verney-Carron; Loryelle Sessegolo; Anne Chabas; Nicolas Nuns; Laurent Remusat; Adriana Gonzalez-Cano; Chloé Fourdrin; Jean-Didier Mertz

Abstract: For a long time, limestone has been massively used in stone building and monuments because of its easy extraction and common presence in the landscape. On ancient monuments, mostly built in urban areas, it is exposed to urban-borne pollutants responsible for specific alteration mechanisms and weathering kinetics. Especially, the dissolution of calcite and the precipitation of new phases will affect the limestone pore network, modify the stones capillary properties and influence the further alteration. In order to better understand these processes, an altered limestone sample from 'Tribunal Administratif' (TA) in Paris was studied. The main secondary phase was found to be syngenite, which can be explained by the location of the sample close to the soil, a potential source of K (fertilizers). This phase is more soluble than gypsum that is commonly found on altered limestone. In order to assess the reactivity of the system (limestone and new phases), oxygen and hydrogen isotopes were used to trace the transfer of water (D218O) and identify the location of the reactive areas (susceptible to alteration). For that, TA samples were exposed in a climatic chamber to relative humidity (RH) cycles (25% RH for 2.5 days and 85% RH for 4.5 days) for 2 months with a D218O vapor to simulate alteration occurring in conditions sheltered from the rain. Results have shown that the water vapor easily circulates deep in the sample and reacts preferentially with syngenite the most reactive phase (compared to calcite and quartz). This phase could evolve in gypsum when exposed to an environment different from the one resulting in its formation.

Suggested Reviewers: Paola Fermo
University of Milan
paola.fermo@unimi.it
Air pollution and monuments
Fermo et al., 2018 (geosciences)

Wolfram Kloppmann

BRGM
w.kloppmann@brgm.fr
limestone, isotopic tracers
Kloppmann et al. 2014 STOTEN

Jose Santiago Pozo-Antonio
University of Vigo
ipozo@uvigo.es
characterization of black crusts
Pozo-Antonio et al. (2017)

Elena Mercedes Perez-Montserrat
Instituto de Geociencias IGEO
empmon@geo.ucm.es
Black layers on limestone and environment
Perez-Montserrat et al., 2016 geosciences

Silvestro A. Ruffolo
Universita della Calabria
silvestro.ruffolo@unical.it
Black crusts and pollution
Ruffolo et al 2015 STOTEN

Opposed Reviewers:

Aurélie VERNEY-CARRON
Laboratoire Interuniversitaire des Systèmes Atmosphériques
61, avenue du Général de Gaulle
94010 Créteil Cedex, France
✉ aurelie.verney@lisa.u-pec.fr

Saint Victor sur Loire, April 20th 2020

Dear Editor,

We would like you to consider the manuscript "**Reactivity of secondary phases in weathered limestone using isotopic tracers (D and ¹⁸O): the case study of the 'Tribunal Administratif' of Paris**" for publication in *Science of the Total Environment*. This manuscript is an original work and has not been submitted for publication in another journal.

The alteration of limestone is a key topic as this sedimentary stone is largely used in historic buildings in Europe and especially in France, whereas it is sensitive to weathering by climate and air pollution. The main alteration features are black crusts in the sheltered areas of the monument and erosion in the unsheltered from rain parts. Whatever the facies, the limestone is porous and undergoes processes of dissolution and precipitation of secondary phases that change the pore network, the petrophysical properties and influence the further alteration.

In this context, this study deals with the characterization of limestone samples from a famous monument in Paris (Tribunal Administratif) weathered for 60 years and the assessment of the reactivity of the system (limestone + secondary phases) when reexposed to a simulated atmosphere by using a D₂¹⁸O vapor. The results show that for studied samples the main secondary phase is syngenite, and not the most common phase usually observed, i.e. gypsum, which can be explained by the capillary rise and the supply of K from soil and fertilizers. The use of an original approach based on isotopes (D and ¹⁸O) and SIMS analyses has also allowed to trace the circulation of water vapor within the sample and locate the reactive zones. D maps have highlighted that water vapor easily circulates in the pore network, whereas ¹⁸O only reacts with syngenite. The change of weathering conditions in the lab experiment compared to the in situ exposure shows that syngenite is not stable and could evolve in gypsum.

We think that this paper fits the aims and scopes of your journal as limestone alteration results here from climatic factors, air pollution and capillary rise from the ground and from dissolution and secondary phase precipitation processes that are controlled by the circulation of liquid water and vapor through the pore network. To investigate these processes are key to better preserve monuments and to assess the impact of the environment, especially in urban areas. Moreover, your journal has previously published very interesting papers dealing with built cultural heritage in calcareous stones (e.g. Kloppmann et al., 2014; Ruffolo et al., 2015; Pozo-Antonio et al., 2017; La Russa et al., 2017). Therefore, we hope that our paper could provide new results to address these questions.

All authors are aware of and accept responsibility for the manuscript.

Yours sincerely,

Aurélie Verney-Carron and coauthors.

1 **Reactivity of secondary phases in weathered limestone using isotopic tracers (D and ¹⁸O): the case**
2 **study of the 'Tribunal Administratif' of Paris**

3
4
5 4 Lucile Gentaz¹, Mandana Saheb¹, Aurélie Verney-Carron¹, Loryelle Sessegolo¹, Anne Chabas¹, Nicolas
6 Nuns², Laurent Remusat³, Adriana Gonzalez-Cano³, Chloé Fourdrin⁴, Jean-Didier Mertz⁵
7
8
9

10 7 ¹ Laboratoire Interuniversitaire des Systèmes Atmosphériques (LISA), UMR CNRS 7583, Université
11 Paris-Est-Créteil, Université de Paris, Institut Pierre Simon Laplace (IPSL), Créteil, France

12 8
13 9 ² Université Lille, CNRS, INRA, Centrale Lille, ENSCL, Université Artois, FR 2638 - Institut Michel-
14 Eugène Chevreul (IMEC), Lille, France

15 10
16 11 ³ IMPMC, Sorbonne Universités, UMR CNRS 7590, UPMC, IRD, MNHN, Paris, France

17 12
18 13 ⁴ Laboratoire Géomatériaux et Environnement (LGE), Université Gustave Eiffel, Marne-la-Vallée,
19 France
20

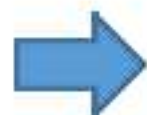
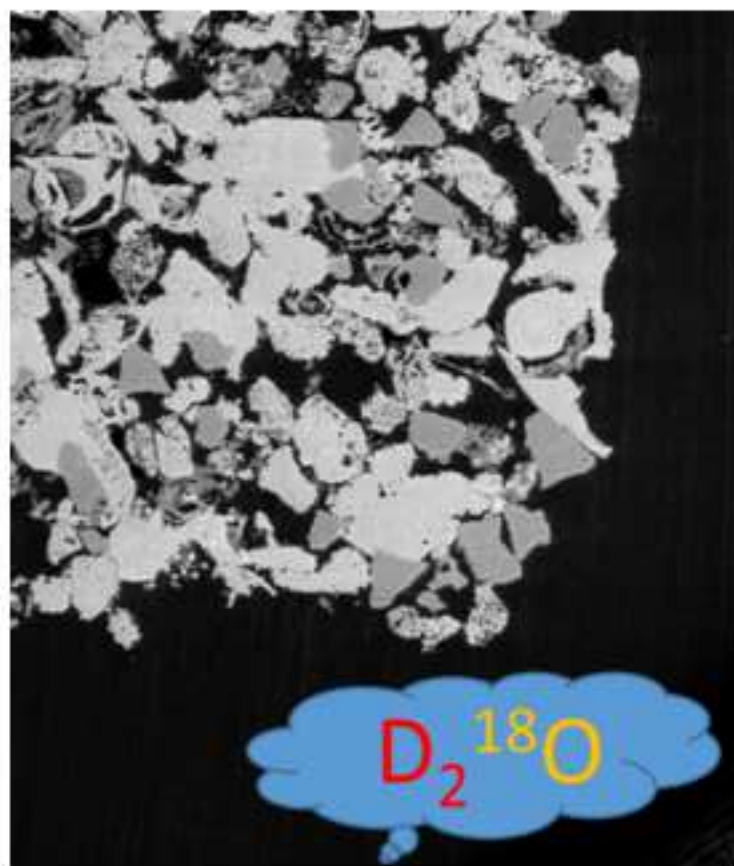
21 14
22 15 ⁵ CRC, Sorbonne Universités, USR 3224 CNRS, MNHN, Ministère de la Culture et de la
23 Communication, CP21, Paris, France

24 16
25 17 ⁶ LRMH, USR 3224, 29 rue de Paris, 77420 Champs-sur-Marne, France
26
27
28
29

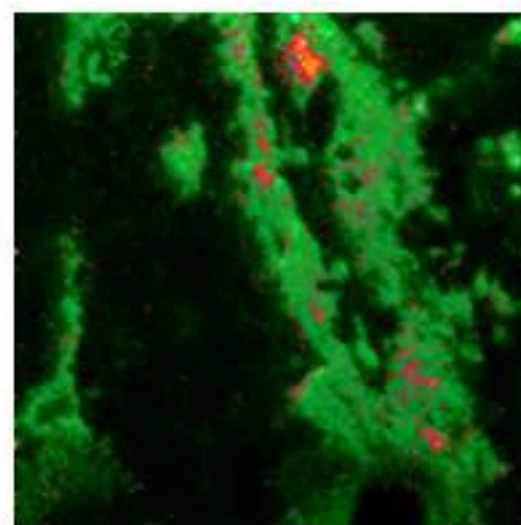
30 **Abstract**

31 For a long time, limestone has been massively used in stone building and monuments because of
32 its easy extraction and common presence in the landscape. On ancient monuments, mostly built in
33 urban areas, it is exposed to urban-borne pollutants responsible for specific alteration mechanisms
34 and weathering kinetics. Especially, the dissolution of calcite and the precipitation of new phases will
35 affect the limestone pore network, modify the stones capillary properties and influence the further
36 alteration. In order to better understand these processes, an altered limestone sample from 'Tribunal
37 Administratif' (TA) in Paris was studied. The main secondary phase was found to be syngenite, which
38 can be explained by the location of the sample close to the soil, a potential source of K (fertilizers).
39 This phase is more soluble than gypsum that is commonly found on altered limestone. In order to
40 assess the reactivity of the system (limestone and new phases), oxygen and hydrogen isotopes were
41 used to trace the transfer of water (D218O) and identify the location of the reactive areas
42 (susceptible to alteration). For that, TA samples were exposed in a climatic chamber to relative
43 humidity (RH) cycles (25% RH for 2.5 days and 85% RH for 4.5 days) for 2 months with a D218O vapor
44 to simulate alteration occurring in conditions sheltered from the rain. Results have shown that the
45 water vapor easily circulates deep in the sample and reacts preferentially with syngenite the most
46 reactive phase (compared to calcite and quartz). This phase could evolve in gypsum when exposed to
47 an environment different from the one resulting in its formation.
48
49
50
51
52
53
54
55
56
57
58
59
60
61
62
63
64
65

**Weathered limestone from the
'Tribunal administratif' of Paris**



SEM-EDS + ToF-SIMS



S (syngenite)
**D (circulation of
vapor in pores)**
 **^{18}O (reactivity
of syngenite)**

150 μm

1.5 mm

HIGHLIGHTS

- Limestone samples from ‘Tribunal Administratif’ of Paris have been characterized.
- In these samples, calcite has been partly transformed in syngenite (K-Ca sulfates).
- Syngenite was formed by reaction with SO₂ and K from capillary rises (fertilizers).
- Water vapor easily circulates within the pore network (D tracing).
- Syngenite is reactive (¹⁸O tracing) and could evolve into gypsum.

36

37 1. Introduction

38 Owing to its ubiquitous presence in the sedimentary landscape and easy extraction,
39 limestone has been largely used in buildings, which raises the question of its preservation and
40 conservation, as limestone is naturally eroded by water. Preserved monuments are often located in
41 urban and polluted areas. Thus, the presence of gas and particulate pollutants in the atmosphere can
42 modify the natural weathering of limestone and the associated kinetics.

43 Limestone is mainly composed of calcite CaCO_3 . It is weathered in the atmospheric
44 environment by meteoritic water through rainfall (runoff) or small water particulate (aerosols) and
45 vapor (relative humidity). Great changes in exposure conditions can take place in the atmospheric
46 environment, with cyclic recurrence of high and low temperature or relative humidity (RH), wet and
47 dry episodes, pollution peaks. Calcite chemical alteration encompasses two processes: calcite
48 dissolution and new phase precipitation. Calcite dissolution is driven by local conditions such as the
49 available water volume, saturation, chemistry (pH, anions and cations concentrations) and
50 temperature (kinetic rates). The pH of the altering solution can be modified by dissolved gas species.
51 Under current CO_2 atmospheric concentration, the pH of meteoritic water (rain droplets) is
52 comprised between 5 and 7 and can induce a karst effect responsible for calcite dissolution
53 (Buhmann and Dreybrodt, 1985; Plummer and Wigley, 1976). Other gaseous pollutants such as SO_2 ,
54 NO_2 and NH_3 , can induce an even greater drop in the rain pH (below pH 5) and are responsible for
55 the phenomenon of acid rain (Bonazza et al., 2009; Smith and Viles, 2006). The dissolution of calcite
56 affects the limestone pore network and can modify the stone capillary properties (Reddy et al.,
57 1986). Moreover, new phase formation can also take place inside or at the surface of the stone and
58 lead to a partial obstruction of the pores, as elements can be dissolved and precipitated again in
59 other parts of the material. The location of these new phases can trace the circulation of water in the
60 pore network. The presence of anions from calcite dissolution or dissolved atmospheric gases in
61 solution leads to the precipitation of carbonates and sulfates (from dissolved SO_2), such as gypsum
62 $\text{CaSO}_4 \cdot 2\text{H}_2\text{O}$ (Sabbioni, 2003; Saheb et al., 2016) and syngenite $\text{K}_2\text{Ca}(\text{SO}_4)_2 \cdot \text{H}_2\text{O}$ (Janssens and Van
63 Grieken, 2004). The precipitation of new phases is especially active on zones sheltered from rain (by
64 roof, cornice or other various relief or sculpted elements) and can be favored by the variability of the
65 hygroscopic conditions in the atmosphere. In sheltered zones, this favors the formation of black
66 crusts (Camuffo et al., 1983; Sabbioni and Zappia, 1992), whereas in unsheltered zones the
67 dissolution leads to erosion and loss of material.

68 As alteration processes influence the evolution of the pore network and the petrophysical
69 properties of limestone, the kinetics of limestone alteration can evolve. Moreover, the secondary
70 phases have a different reactivity. The cyclic nature of the atmospheric medium implies that

71 alternating dissolution and precipitation episodes will repeat on a material constantly changing and
72 further and further altered. Therefore, to understand alteration mechanisms of weathered
73 limestone, it is essential to identify the secondary phases and determine their reactivity.

74 In this context, the purpose of this work is to understand the fine scale processes taking place
75 during the atmospheric weathering of monumental limestone. This study focuses on the alteration
76 occurring in conditions sheltered from the rain and resulting solely from the action of water as vapor.
77 Indeed, in those conditions, since run-off should not occur, calcite, ions and most of the dissolved
78 elements will remain on the original sample.

79 In order to follow the transfer of water vapor inside the limestone and its reactions with the
80 substrate, whilst providing information on the location of the reactive areas, experimental
81 weathering of ancient building stones was conducted using $D_2^{18}O$. The use of these isotopic tracers
82 provides information on both the depth of the water penetration front and specific reactive zones in
83 the substrate. Indeed, deuterium can be linked to adsorption processes, as it is likely to form weak
84 hydrogen-bonds with the substrate. Deuterium location can be therefore seen as the tracer of the
85 water penetration front. For ^{18}O to remain in a dry sample after the experiment, stronger bounds are
86 required. This oxygen isotope is itself a tracer of alteration and precipitation reactions occurring in
87 the limestone. This identification calls for an isotope analytical technique with sensitivity ranging
88 from the micrometer to the nanometer. In order to obtain in depth information, up to several
89 millimeters, cross sections of the samples were made and subsequently analyzed. Two isotopic
90 investigation methods were used: NanoSIMS and ToF-SIMS, both based on Secondary Ion Mass
91 Spectrometry and sharing capabilities of high spatial resolution imaging.

92

93 **2. Materials and methods**

94

95 *2.1. Samples*

96

97 Many historical Paris monuments in Paris are characterized by limestone from the Paris
98 Basin. One specific type of limestone was chosen for this study, the "*Saint-Maximin roche fine*"
99 formed during Lutetian age (45 My). This stone is often used for the restoration of historical
100 monuments for its easy shaping and its physical and mechanical properties. "*Saint-Maximin roche*
101 *fine*" is a chemically homogeneous rock composed originally of *ca.* 95% of $CaCO_3$ and 5% of SiO_2 .
102 Porosity, sorption and hygroscopic properties and evaporation, have been explored in previous work
103 (Chabas et al., 2018; Saheb et al., 2016).

104 The chosen sample is an altered sample from 'Tribunal Administratif' in Paris, a pre-
105 haussmannian monument originally built in the 17th c. This sample, referred to as "TA", was part of a

106 restoration stone block dating to the 20th century (ca. 1950) and has been therefore altered for more
107 than 60 years. The retrieved sample was collected at 1m above ground, thus subjected to capillary
108 rising (Saheb et al., 2014).

109

110 *2.2. Isotopic labelling experiment*

111

112 To investigate the alteration mechanisms induced on limestone by water vapor, a
113 methodology based on the use of D₂¹⁸O water was applied (Saheb et al., 2015). The sample was
114 submitted to a series of humidity cycles with water vapor doped in D and ¹⁸O, in controlled
115 conditions, in order to reproduce variations of RH found in atmospheric outdoor sheltered
116 conditions.

117 The original limestone sample was divided into 5 cm-long rods with a 1x1cm² section. To
118 reproduce the exposure conditions of a stone block on a building façade, only one face
119 (perpendicular to the length) was exposed to the environment. The other sides were shielded by an
120 aluminum foil. For 61 days (2 months), the limestone was exposed in the CIA (Chamber for Isotherm
121 Adsorption) regulated at 20 ± 1°C and iteratively and alternatively placed inside desiccators whose
122 RH was controlled by supersaturated saline solution at 25% RH (for 2.5 days) and at 85% RH (for 4.5
123 days). Solutions of CH₃COOK and K₂SO₄ were used to set relative humidity at 25% and 85%,
124 respectively. In both cases, the water vapor present in the desiccators was enriched in deuterium,
125 90% of all hydrogen nuclei, and oxygen 18, 10% of all oxygen nuclei; with regards to water molecules,
126 18 D nuclei for every ¹⁸O nucleus. Residual traces of these isotopes present in the samples should
127 indicate the location of the reactive alteration zones inside the materials. After the experiment,
128 samples were kept in a desiccator (14% RH) to prevent further alteration. The samples were then cut,
129 imbedded in resin and their surface polished using SiC discs and for finer grind velour discs and
130 diamond suspensions down to 0.25 µm.

131

132 *2.3. Analytical techniques*

133

134 *2.3.1. Chemical characterization.* Preliminary observations of the samples were conducted on
135 polished sample cross sections imbedded in resin, up to 2 mm in depth. Morphological and chemical
136 surveys of the samples were led in order to locate the areas of interest, using a Zeiss ULTRA55 SEM
137 using a FEG-Schottky electron gun. The images were acquired at 15 kV. The SEM is equipped with
138 energy dispersive spectrometer Quantax (Bruker). Elements of interest were mapped using the EDS:
139 K, Si, C, Ca, O and S. Preliminary mineralogical surveys of the alteration phases were carried out
140 through Raman spectrometry, using a Renishaw InVia spectrometer equipped with a 532 nm NdYAG

141 laser source and a Leica microscope. Reference spectra were obtained through RRUFF database
142 (Buzgar et al., 2009; Gunasekaran et al., 2006).

143

144 *2.3.2. Isotopic analyses.* In order to understand the general make-up of isotopic composition of the
145 first millimeters of the sample, ToF-SIMS analyses were conducted. ToF-SIMS spectra measurements
146 were carried out using an IONTOF TOF.SIMS⁵ (GmbH, Germany) instrument. This machine is
147 equipped with a Bismuth (25keV) source for analysis and a cesium source for sputtering. Before each
148 500X500 μm^2 analysis, surface was sputtered with Cs^+ at 2 keV over a $750 \times 750 \mu\text{m}^2$ areas for ca.
149 20 min, to remove surface contamination.

150 Acquisition were performed in negative polarity using burst mode 6 pulses to avoid 1H^- and
151 16O^- detector saturation and to obtain both good lateral resolution ($\approx 200 \text{ nm}$) and mass resolution
152 ($m/\Delta m > 5000$ at $m=16$ for oxygen). $500 \times 500 \mu\text{m}^2$ areas were analyzed (256×256 pixels) in a row
153 from the surface to 1.85 mm inside the sample. Smaller regions of interest ($150 \times 150 \mu\text{m}^2$) inside
154 these larger areas were subsequently mapped in order to identify more specifically the location of
155 isotopic enrichments.

156 Data post-treatment allowed us to finely calculate deuterium and ^{18}O concentration over
157 large area from sample surface to 1.85mm inside. For D/H ratio, calculation can be done directly
158 from peaks corrected intensity at $m/z=1$ and $m/z=2$. $^{18}\text{O}/^{16}\text{O}$ ratio calculations were more challenging
159 since mass resolution was not sufficient to avoid overlapping of $^{18}\text{O}^-$ ($m/z=17.9992$) with $^{16}\text{OD}^-$
160 ($m/z=18.009$) and $^{16}\text{OH}_2^-$ ($m/z=18.0106$). These overlapping are represented in Fig. 1a. The first peak
161 corresponds to ^{18}O and the second peak corresponds to the signal of both D^{16}O and H_2^{16}O . These two
162 hydrogen-containing species are closer in mass ($1.5 \cdot 10^{-3} \text{ u}$ distance) and could not be discriminated
163 efficiently given the mass resolution.

164 The treatment of the pulsed burst, in order to enhance the intensity of the collected signal,
165 was implemented based on the work of (De Souza and Martin, 2008). In this previous study, the
166 authors added the first individual pulse to itself 6 times in order to enhance the signal from the 18u
167 region. Only the first burst was selected in order to neutralize the phase shift observed in the
168 subsequent bursts. This enhanced the signal but the background noise as well. In the present study,
169 the pulsed burst provided 6 individual pulses (Fig. 1a) of very similar periods: $0.0620 \pm 0.0006 \text{ u}$
170 around 18 u. The choice was made to sum up the intensity count from each pulse, due to the limited
171 shift in the period observed for each pulse. This provided a meta-signal presenting a smaller noise to
172 signal ratio (Fig. 1b). A subsequent deconvolution of the signal was undertaken using the software
173 Origin 8. The meta-signal was fitted, using Gaussian functions (high symmetry for the peaks) to fit
174 each individual species (D^{16}O , H_2^{16}O and ^{18}O) to the signal (Fig. 1c). Using the calculated area of each

175 peaks, A_{18O} / A_{tot} ratio were calculated in order to assess the individual contribution of ^{18}O to the
176 signal. The isotopic intensity count was then corrected by this ratio.

177 The identification of the reactive areas at the grain-interface (on the surface or inside the
178 bulk) requires a finer mapping grid. Similar studies on the water vapor circulation have been
179 successful at identifying these reactive areas on glass using NanoSIMS (Sessegolo et al., 2018). These
180 regions of interest were studied at the submicron-scale using a Cameca NanoSIMS (Secondary Ion
181 Mass Spectrometry) NS50 operated at the National Museum of Natural History in Paris (MNHN Paris)
182 using a 16 keV primary Cs^+ beam. Secondary ions were collected in multicollection mode.
183 Quantitative images covering surface areas of $20 \times 20 \mu m^2$, divided into 256 by 256 pixels were
184 acquired at a raster speed of 1ms/pixel. In order to map D/H and $^{18}O/^{16}O$, we recorded the
185 distribution of H^- and D^- on the one hand, and then $^{16}O^-$, $^{18}O^-$, $^{28}Si^-$ and $^{32}S^-$ on the second hand.
186 Contrary to ToF-SIMS, no treatment was needed to discriminate $^{18}O^-$ from $D^{16}O$ and $H_2^{16}O$ with
187 NanoSIMS, due to its sufficient mass resolution. An electron flooding gun was used to offset charge
188 effects. Before, each analysis, the sample surface was presputtered over $25 \times 25 \mu m^2$ surface area with
189 a current of 650 pA for about 20 minutes in order to remove surface contamination and to reach a
190 steady-state sputtering (Thomen et al., 2014). $^{16}O^-$, $^{18}O^-$, $^{28}Si^-$ and $^{32}S^-$ were analyzed in a first session
191 with a primary beam current of 1.5 pA. Then D^- and H^- images were acquired at the exact same
192 location during a second session of image acquisitions with a 50 pA beam current for analysis. Ratio
193 maps were calculated for hydrogen and oxygen isotopes using the L'IMAGE software developed by
194 Larry Nittler (Carnegie Institution in Washington DC, USA). This image processing included a stage of
195 co-registration of multiple frames to account for drift in the location of the ion beam from frame to
196 frame.

197

198 **3. Results**

199

200 *3.1. Identification of the altered phases*

201

202 Before the experiment, the sample of the Tribunal Administratif – weathered for more than
203 60 years – displayed the presence of alteration phases up to a depth of 6 mm below the surface.
204 Most of these phases were concentrated within the first 2 mm underneath the surface. *Saint-*
205 *Maximin roche Fine* limestone can be classified as a grainstone and a biosparite (Dunham, 1962; Folk,
206 1959). In the case of TA sample, the alteration has somewhat modified the original limestone. These
207 altered samples are characterized by the presence of large angular bioclastic fragments (up to 500
208 μm in length) and rounded quartz grains (50 to 200 μm in diameter) typical of the limestone. A finer
209 section, more akin to micritic fragments, is present. These fine grains are located around the grains

210 and pores and correspond to the alteration phases. TA samples porosity was relatively high, 43.0 ± 0.2
211 % (Saheb et al., 2014), but still in the range observed for this type of limestone.

212 After a two-month exposure to the RH cycles, SEM-EDS mapping of an in-depth section of the
213 sample shows the presence of elements characterizing limestone. The presence of Ca was somewhat
214 ubiquitous in the sample (Fig. 2a orange), inherent to the calcite rich substrate (limestone), with two
215 exceptions: areas presenting high relative concentration of Si (Fig. 2a blue) and O most likely
216 associated most likely to quartz grains, and areas characterized by the presence of C and O mostly
217 associated with the resin filling pores (Fig. 2a black). In some of these Ca-containing areas, the
218 concentration of said element was relatively lower and accompanied with the presence of S (Fig.
219 2a,b). Sulfur is not inherent to the original limestone; it is the evidence of the presence of exogenous
220 deposition inside the material, showing the influence of gaseous pollutant SO_2 . EDS mapping also
221 shows the quasi ubiquitous presence of K (Fig. 2c) in the sulfur enriched areas (Fig. 2b). Therefore, S-
222 enriched areas could correspond to the presence of syngenite (for K, Ca and S) and/or gypsum (for Ca
223 and S).

224 Raman spectra were collected in order to identify the alteration phases present in depth
225 underneath the sample surface in areas enriched in sulfur (Fig. 3). On TA sample exposed 2 months,
226 well-defined peaks were observed at 984, 1008 and 1085 cm^{-1} on some spectra. The peak at 1085
227 cm^{-1} is very characteristic of calcite (Gunasekaran et al., 2006), the other peaks can both be
228 associated to syngenite (Buzgar et al., 2009). The presence of gypsum cannot be ruled out since its
229 main peak around 1007 cm^{-1} coincides with the second peak of syngenite. Therefore, TA samples
230 presented a mixture of several minerals including calcite, syngenite and possible gypsum (Fig. 3a).
231 The presence of ^{18}O isotopes can be associated with shifts in the Raman peaks (Perdikouri et al.,
232 2013). In TA samples, no significant shifts were observed in the Raman peaks compared to the
233 reference. This would suggest that tracer isotopes were not present in high concentrations in the
234 identified minerals. Another Raman spectrum, obtained on a TA sample exposed 1 year presents
235 peaks corresponding to calcite (1085 cm^{-1}) and to salts containing K and S respectively: niter – KNO_3
236 (1053 cm^{-1}) and thenardite – NaSO_4 (994 cm^{-1}) displaying a slight shift from the references of 1048
237 cm^{-1} and 989 cm^{-1} respectively observed in (Morillas et al., 2015). These minerals can be added to the
238 list of sulfates and carbonates identified at 2-month exposure (Fig. 3).

239

240 3.2. Penetration of heavy isotope enriched vapor

241

242 The penetration of D_2^{18}O enriched water cannot be monitored directly during the experiment
243 but the presence of D and ^{18}O can be observed in the sample afterwards using SIMS instruments.
244 Traces of these isotopes in the sample were found after the experiment in concentration superior to

245 their natural abundance. The D/H and $^{18}\text{O}/^{16}\text{O}$ ratios were calculated for the first 2 mm in depth
246 inside the TA sample using ToF-SIMS maps. These isotopic maps (Fig. 4) correspond to the area
247 presented in Fig. 2 and corresponding to previously acquired EDS maps.

248 Average isotope count over the analytical areas of $500 \times 500 \mu\text{m}^2$ was used to calculate
249 ratios. In addition, for the first millimeters below the surface, regions of interest (ROI) were created
250 in the maps, allowing for the calculation of average isotopic count over smaller sections of $250 \mu\text{m}$ in
251 depth by $500 \mu\text{m}$ in width. These average values were compared to natural abundance of deuterium
252 (Fig. 5).

253 A very high concentration of D was found directly on the surface, and registered between
254 1.19×10^{-3} and 3.74×10^{-3} further inside the sample (10 to 30 times above the natural ratio of 1.5×10^{-4})
255 (Table 1). This observation confirms that D remained in the sample after the experiment and
256 interacted with substrate. This infers that water vapor has diffused throughout the entire sample.
257 This was corroborated by punctual NanoSIMS measurements in depth in the sample.

258 Higher concentrations of ^{18}O were found near the surface (Fig. 5) (1.29 times above the
259 natural ratio of 0.0020), with a progressive decrease in depth in the sample. The concentration
260 gradient observed for the oxygen isotope between the surface and the samples depth suggests a
261 progressive effect of the isotopic exchange (Table 1).

262 NanoSIMS mapping of D/H and $^{18}\text{O}/^{16}\text{O}$ ratios in TA samples was conducted as well on
263 smaller areas of interest in the sample. NanoSIMS was chosen to investigate specific areas more
264 prone to exhibit heavy isotope enrichments. Similar to ToF-SIMS, the enrichment ratio was calculated
265 using the average isotopic count over each NanoSIMS map. The maps correspond to $20 \mu\text{m}$ by $20 \mu\text{m}$
266 areas.

267 The comparison of the deuterium ratio to the natural abundance provides information on the local
268 enrichments in the reactive areas of the sample (Table 1). The studied areas of interest studied
269 showed the deuterium concentration in these specific areas could reach 900 times the natural ratio,
270 with a median value over the 7 studied areas of 0.0264 (230 times the natural ratio) (Table 1). In the
271 case of ^{18}O , the local enrichments could reach 1.76 times the natural ratio, with a median value over
272 the 7 studied areas of 3.52×10^{-3} (1.89 times the natural ratio) (Table 1).

273 Comparing the two SIMS techniques, the enrichments calculated on the smaller areas of
274 interest with NanoSIMS results register an order of magnitude above ToF-SIMS ratio for D. Ratios
275 were very similar for the two techniques for ^{18}O , although slightly superior for NanoSIMS. One should
276 note that the values obtained for each technique are averaged over different surface, with a higher
277 dilution of the signal for the larger areas analyzed with ToF-SIMS. NanoSIMS, on the contrary,
278 provides information on smaller areas of interest displaying higher isotopic concentrations and
279 where more reactions are expected to have occurred.

280

281 3.3. Identification of the reactive zones

282

283 The identification of the phases throughout the sample showed the presence of calcite,
284 quartz and syngenite (Fig. 3). ToF-SIMS maps of an area of interest are presented in Fig. 6. These
285 maps show that the locations of ^{18}O and D high enrichment zones are identical. These two elements
286 are most likely correlated here in the structure. When comparing the regions enriched in ^{18}O and D
287 on Fig. 6, these zones correspond to phases enriched in S, most likely corresponding to syngenite
288 evidenced in Raman spectrometry. On a larger scale, a more systematic comparison can be made
289 between the areas on Fig. 4 and the EDS maps on Fig. 3, where enriched region corresponds to K and
290 S containing areas.

291 NanoSIMS maps were used to identify the specific reactive areas at a finer scale. Results
292 show punctual enrichment in (Fig. 7) both D and ^{18}O located in S-rich alteration phases, but none
293 located in the resin (characterized by ^{12}C) or quartz grains (characterized by ^{28}Si), as already observed
294 in ToF-SIMS (Fig. 6). The reactive area is up to 4 μm in thickness. It is located on the edge of the
295 alteration phase (right side of the maps), in contact the quartz grain and the pore (left side of the
296 maps). The information provided by nano-scale observation shows that reactive areas are located
297 either at the grain boundary or on the surface of the pores where water vapor can come directly in
298 contact with the alteration phase.

299

300 4. Discussion

301

302 4.1. Specificity of the TA sample

303

304 The alteration phases present in TA sample before the study are somewhat different from
305 the usual phases observed in similar objects (Saheb et al 2013, Saheb et al 2016). Whereas gypsum is
306 the main secondary phase usually found on limestone exposed to an urban area (Saheb et al, 2016;
307 Camuffo et al, 1983), the TA sample is enriched in K (Fig. 2 c). The presence of this element has been
308 associated with the precipitation of syngenite ($\text{K}_2\text{Ca}(\text{SO}_4)_2 \cdot \text{H}_2\text{O}$) in the sample (Fig. 3). In literature,
309 potassium-rich phases observed on the surface of limestone have been associated to the presence of
310 an organic source in the atmosphere or in the soil (Matović et al., 2012). In an urban area, potassium
311 rich salts on cultural heritage buildings have been associated to the presence of pigeon droppings
312 (Gomez-Heras et al., 2004) or linked to the deposition of biomass burning particles (Frenay et al.,
313 2009). The high K concentration observed in TA samples is most likely to come from a
314 complementary source as well. TA sample was collected in an area of the building close to the

315 ground (c.a. 1m above ground). At this elevation, the stone is subjected to capillary rise. In this case,
316 a non-atmospheric source of potassium is very likely to be the soil. Since the building is located in an
317 urban area, the source of organic material is most likely be associated to punctual use of chemical
318 fertilizer (KNO_3) on the few grass-beds present around the building but can also be associated to the
319 presence of pigeon droppings. Indeed, Raman analyses (Fig. 3) of a separated TA sample (exposed 1
320 year to the vapor) presented traces of niter (KNO_3) as well as thenardite, a fairly common salt in
321 altered porous limestone (Doehne et al., 2002; Rodriguez-Navarro et al., 2000; Shahidzadeh-Bonn et
322 al., 2010).

323

324 4.2. Isotope interactions with the sample

325

326 When the D_2^{18}O enriched water penetrates into the sample, it interacts with the surface of
327 the accessible grains, either at the grain boundary or in the open porosity (Fig. 7). Measurements
328 obtained with the two different SIMS techniques showed general increase in the isotopic ratio (fD
329 and $f^{18}\text{O}$) throughout the sample. These isotopic fractions are relatively similar according the SIMS
330 technique and small differences can be explained by the difference of data treatment (see 2.3.2). The
331 overall penetration of the water vapor in the porous system confirms that interaction between water
332 and limestone can occur during the dry period and that the alteration, although at different
333 intensities, could be occurring not only during the rainfall events but almost continuously. The depth
334 of the vapor penetration could also infer that the risk areas are not limited to the sub-surface alone
335 but could take place further inside the stone. Nevertheless, these enrichments differ between ^{18}O
336 and D, with ratio always greater fD for than $f^{18}\text{O}$, due to different original enrichment in solution for
337 the two species (Table 1).

338 In the TA samples, the enrichment factors of the tracer isotopes vary as well. This can be in
339 part explained by the enrichment in the water vapor, as the deuterium enrichment is 90% of the
340 total hydrogen but the oxygen 18 correspond to only 10 % of the oxygen. The enrichments observed
341 in the TA samples are both very inferior to the ones measured in the alteration solution. Therefore,
342 these results in sample were compared to the natural abundance ratios of the isotopes and not the
343 alteration solution. ToF-SIMS shows a 10- to 30-fold enrichment in D compared to the natural
344 abundance, whereas the ^{18}O enrichment was only 1.07 to 1.27 the natural abundance (Table 1). For
345 NanoSIMS as well, D enrichment is greater than ^{18}O enrichment. Looking at $\text{D}/^{18}\text{O}$ ratios (Table 1),
346 sample enrichments are very different from the ones measured for the alteration solution. The
347 discrepancy in the enrichment could therefore indicate that the two elements present in solution
348 might not interact in the exact same way with the sample.

349 Water vapor can firstly form a hydrated layer adsorbed onto the surface of the pores.
350 Deuterium forms Van der Waals forces with the surface site hydrogen. These surface sites can be
351 enriched in deuterium up to the point where they are all saturated forming an enriched hydrated
352 layer at the pores and minerals surface. Therefore, the presence of deuterium in the newly altered
353 samples is an effective tracer of the depth of the water vapor penetration. Since the samples were
354 kept in a dry environment (desiccator) after alteration and analyses were performed in vacuum
355 chamber, most adsorbed residual water has been removed from the sample. However, despite the
356 desorption induced by the experiments, a significant D enrichment remains. Indeed, during the
357 experiment and to a lesser extent afterwards, isotopic exchange can occur between the hydrogen
358 present on the surface of the minerals and the deuterium in the hydrated enriched layer (Sessegolo
359 et al., 2018). The presence of ^{18}O in the sample can be also related either to the presence of residual
360 water or to the presence of newly precipitated phases resulting in interactions between the
361 substrate and the vapor. ^{18}O found in the samples can be considered as a tracer of interactions
362 between the substrate and the vapor.

363 In most cases, ^{18}O and D can be found in the same location (Fig. 4, 6, 7). The conjoined
364 presence of these two species in ratios comparable to their original vapor concentration could
365 indicate that the isotopes are present under the D_2^{18}O form in the reactive species. Syngenite (K_2
366 $\text{Ca}(\text{SO}_4)_2 \cdot \text{H}_2\text{O}$), the reactive phase, is a hydrated mineral and the substitution of ^{16}O for ^{18}O can occur
367 in the molecular H_2O or in the sulfate. In the present case, the simultaneous presence of ^{18}O and D
368 shows that the integration of the isotopes to the sample has occurred in the syngenite molecular
369 water, with a newly formed enriched syngenite: $\text{K}_2\text{Ca}(\text{SO}_4)_2 \cdot \text{D}_2^{18}\text{O}$. A similar result should be
370 expected, on gypsum precipitates that could be present in the sample ($\text{CaSO}_4 \cdot 2\text{D}_2^{18}\text{O}$).

371 In parallel to this general case, small differences can occur here and there. On Fig. 4 a large D
372 enriched area can be observed at 100 μm below the surface (vertically centered) but is far less
373 reactive for ^{18}O . These variations could account for the discrepancy with the original vapor found in
374 some cases with ToF-SIMS, with greater deuterium enrichment and could correspond mainly to
375 sorption of water without significant reaction. On Fig. 7 conversely, on the lower left of the reactive
376 area, ^{18}O is present where D enrichment is tenuous. This specific area could be the location of a
377 different molecular substitution. Indeed, a substitution in carbonate or sulfate molecules can be
378 traced by the presence of ^{18}O alone. In this area, the relative absence of deuterium could infer the
379 integration of ^{18}O in SO_4^{2-} . The presence of marked sulfate could be indicating of the precipitation of
380 new alteration phase during the experiment, but the nature of this new sulfate-rich phase was not
381 specifically identified: syngenite, gypsum or thenardite (Fig. 3).

382

383 *4.3. Reactivity of the different phases*

384

385 Comparing the information provided by Fig. 2 and Fig. 4, isotope tracers have not been
386 observed in areas corresponding to quartz grains or purely calcite grains. Syngenite was identified as
387 the main reactive phase in TA sample and is more likely to be altered again in the future. The
388 dissolution of syngenite occurs preferentially to the dissolution gypsum or calcite. Syngenite
389 solubility is $8.3 \text{ mmol} \cdot \text{L}^{-1}$ (Darvell, 2018) and higher than gypsum which is $4.9 \text{ mmol} \cdot \text{L}^{-1}$ ((Colombani,
390 2008); $K_s = 5 \cdot 10^{-5}$) or calcite, $0.06 \text{ mmol} \cdot \text{L}^{-1}$ ((Visconti et al., 2010); $K_s = 3 \cdot 10^{-9}$). Furthermore, the
391 lack of Raman signal in highly altered areas suggests that the altered phases are not as well
392 crystallized as calcite or quartz grains and their grain size is generally smaller. For a similar volume of
393 mineral, smaller syngenite grains possess a greater specific surface and therefore a greater reactive
394 surface area. This morphological difference can influence the preferential alteration of syngenite.

395 The ubiquitous presence of syngenite in the TA sample is associated with a large source of
396 potassium in the system, stemming from an organic source and influenced by the capillary rise from
397 the soil. If we consider the future evolution of similarly altered limestone, one fundamental question
398 is: are these specific alteration phases stable once the local potassium source is removed? For the
399 experiment in isotopically labelled water vapor, the samples have been removed from the local
400 source of potassium present at the base of the TA building. In new environmental conditions, the
401 syngenite is not at equilibrium with its surroundings. The main interaction between the vapor and
402 the sample after two-month exposure is a substitution in the hydrated molecule of syngenite, but
403 evidence was found that new sulfate phase might have precipitated as well (Fig. 7). Since NanoSIMS
404 analyses monitored sulfur but not potassium or calcium, and Raman analyses did not provide
405 sufficient lateral resolution for these small phases, it is unclear if the new precipitate is syngenite.

406 Using CHES thermochemical code (van der Lee and De Windt, 2002) in association with
407 “Thermo-chimie” database, calculations were carried out to trace the evolution of syngenite in a
408 solution with a composition similar to rainwater. When increasing the potassium concentration in
409 the solution in comparison to typical rain composition, the syngenite remained. In typical rain
410 conditions (no additional potassium), the syngenite was partially replaced by gypsum. This
411 replacement of syngenite by gypsum in an environment only influenced by rain water composition
412 shows that the presence and conservation of syngenite in the sample is inherent to the local
413 condition to which it is exposed in the building.

414 If the local environmental conditions change in the building, the syngenite is likely to react to
415 form new alteration phases, most likely gypsum. Since the dissolution of syngenite will occur
416 preferentially it can be inferred that this phase will be progressively replaced.

417

418 *4.4. Estimation of the reaction rate*

419

420 Mercury intrusion porosity (MIP) measurements have already been performed on ancient
421 samples from the study frame (Saheb et al., 2016). The value of the specific surface area for TA
422 before vapor alteration is of $0.22 \text{ m}^2 \cdot \text{g}^{-1}$ (Saheb et al., 2015). Surface analyses were conducted using
423 Histolab[®] software on large SEM images (Fig. 2) obtained at a resolution of $0.74 \text{ }\mu\text{m}$ per pixel. This
424 resolution did not allow for an accurate evaluation of the specific surface, but the values calculated
425 via Histolab[®] were in the same order of magnitude as mercury porosity measurements (2.3 times
426 lower than MIP). This surface estimation allowed for an approximation of relative contribution of
427 each phase to the specific surface of the sample. Quartz grains contributed to 0.5 % of the surface
428 area, calcite contributed to 82.5% of the surface area and sulfur-containing alteration phases
429 (syngenite) contributed to 17% of the surface area. Relatively to the specific surface area measured
430 via MIP, the specific surface area of the reactive phases, *e.g.* the sulfur-containing alteration phases,
431 is about $0.04 \text{ m}^2 \cdot \text{g}^{-1}$.

432 On the NanoSIMS analyses, the thickness of the reactive mineral reached up to $4 \text{ }\mu\text{m}$ in
433 thickness (Fig. 7) but was only present in limited sections of the surface of the alteration phase. Using
434 the same surface analyses technique on large ToF-SIMS images (Fig. 4), the zones enriched in ^{18}O and
435 D were estimated to represent 31% of the potential reactive phase volume. Taking into account the
436 maximum thickness of $4 \text{ }\mu\text{m}$ for these reactive areas, an average surface of 0.01 mm^2 can be
437 estimated for the reactive areas, as well as the specific surface area for enriched phase of 0.004
438 $\text{m}^2 \cdot \text{g}^{-1}$. Given that the substitution of H_2O by D_2^{18}O has been shown to occur at the mineral surface
439 (in the pores or at grain boundary), the specific surface area provides information on the rate of
440 substitution. Comparing this specific surface area for enriched phase with syngenite phase specific
441 surface area, substitution occurred on 10% of syngenite phase after two-month exposure to water
442 vapor. This rate corresponds to the isotopic exchange rate of H and O atoms in the syngenite.
443 However, it highlights that even if the exposure is short, the syngenite is highly reactive with the
444 water vapor and that the system (limestone and new phases) can rapidly evolve.

445

446 5. Conclusion

447

448 The study of an altered limestone sample from 'Tribunal Administratif' in Paris has shown the
449 alteration phases already present are the result of a very specific environment, enriched in
450 potassium. Contrary to many similar samples where gypsum is the main alteration phase, TA sample
451 main alteration phase is syngenite. This phase reflects the presence of a very specific pollution source
452 in the sample immediate surrounding and the influence of capillary rising on building limestone close

453 to the ground. Modifications in the limestone environment are responsible for the evolution of the
454 alteration phases.

455 The use of isotopic labels has allowed for the identification of reactive areas in the sample more
456 likely to be altered again. The use of high concentration of ^{18}O studied via ToF-SIMS was key in the
457 implementation of a new methodology of signal treatment that allowed for the specific
458 quantification of species presenting very similar atomic mass. This new methodology allowed for the
459 accurate calculation of the oxygen isotopic ratio even in highly hydrated areas.

460 When studying this system using isotopically labelled vapor, syngenite was found to be the
461 main reactive phase. The larger part of the isotopes is integrated into the sample under the D_2^{18}O
462 form by substitution in the syngenite molecular water. There is nevertheless some evidence that ^{18}O
463 was present without D in some alteration phases, suggesting its integration to sulphates, most likely
464 through the precipitation of new alteration phase in the system.

465 This new phase precipitation happened in an environment presenting a very specific
466 unforeseen difference in composition to the original location of the sample. Thermodynamic
467 calculations have shown that the syngenite could be replaced by newly formed gypsum in such a
468 case. This example is key to understand the evolution of altered material faced with evolution in its
469 environment.

470 Considering the field of heritage material conservation, key pieces of material can be
471 transferred from one environment to another. Here, we see that a modification of the concentration
472 of one specific element can impact the reactivity of the alteration phases present in the object.
473 Therefore, to ensure the durability of the material, any drastic change in the object direct
474 environment should be limited as much as possible or heavily monitored.

475

476 **Acknowledgements**

477 The authors would like to thank the French National Research Agency (ANR) for their financial
478 support (ANR GLAM). The NanoSIMS Facility at MNHN was funded by CNRS, Région Île de France,
479 Ministère délégué à l'Enseignement supérieur et à la Recherche and MNHN.

480

481 **References**

- 482 Bonazza, A., Messina, P., Sabbioni, C., Grossi, C.M., Brimblecombe, P., 2009. Mapping the impact of
483 climate change on surface recession of carbonate buildings in Europe. *Science of The Total*
484 *Environment* 407, 2039–2050. <https://doi.org/10.1016/j.scitotenv.2008.10.067>
- 485 Buhmann, D., Dreybrodt, W., 1985. The kinetics of calcite dissolution and precipitation in geologically
486 relevant situations of karst areas: 1. Open system. *Chemical Geology* 48, 189–211.
487 [https://doi.org/10.1016/0009-2541\(85\)90046-4](https://doi.org/10.1016/0009-2541(85)90046-4)
- 488 Buzgar, N., Buzatu, A., Sanislav, I.V., 2009. The Raman study of certain sulfates. *Analele Stiintifice ale*
489 *Universitatii Al. I. Cuza Iasi - Geologie* 55, 5–23.

490 Camuffo, D., Del Monte, M., Sabbioni, C., 1983. Origin and growth mechanisms of the sulfated crusts
491 on urban limestone. *Water Air Soil Pollut* 19, 351–359. <https://doi.org/10.1007/BF00159596>
492 Chabas, A., Sizun, J.-P., Gentaz, L., Uring, P., Phan, A., Coman, A., Alfaro, S.C., Saheb, M., Pangui, E.,
493 Zapf, P., Huet, F., 2018. Water content of limestones submitted to realistic wet deposition: a
494 CIME2 chamber simulation. *Environ Sci Pollut Res* 25, 23973–23985.
495 <https://doi.org/10.1007/s11356-018-2433-0>
496 Colombani, J., 2008. Measurement of the pure dissolution rate constant of a mineral in water.
497 *Geochimica et Cosmochimica Acta* 72, 5634–5640.
498 <https://doi.org/10.1016/j.gca.2008.09.007>
499 Darvell, B.W., 2018. Gypsum Materials, in: *Materials Science for Dentistry*. Woodhead Publishing
500 Series in Biomaterials, pp. 40–69.
501 De Souza, R.A., Martin, M., 2008. Using 18O/16O exchange to probe an equilibrium space-charge
502 layer at the surface of a crystalline oxide: method and application. *Phys. Chem. Chem. Phys.*
503 10, 2356–2367. <https://doi.org/10.1039/B719618K>
504 Doehne, E., Selwitz, C., Carson D.M., 2002. The damage mechanism of sodium sulfate in porous
505 stone., in: *Proceedings of the SALTeXPert Meeting*. Presented at the ARCCHIP, Prague, pp.
506 127–146.
507 Dunham, R.J., 1962. Classification of Carbonate Rocks According to Depositional Textures, in:
508 *Classification of Carbonate Rocks*. AAPG Special Volumes, pp. 108–121.
509 Folk, R.L., 1959. Practical Petrographic Classification of Limestones. *AAPG Bulletin* 43, 1–38.
510 <https://doi.org/10.1306/0BDA5C36-16BD-11D7-8645000102C1865D>
511 Freney, E.J., Martin, S.T., Buseck, P.R., 2009. Deliquescence and Efflorescence of Potassium Salts
512 Relevant to Biomass-Burning Aerosol Particles. *Aerosol Science and Technology* 43, 799–807.
513 <https://doi.org/10.1080/02786820902946620>
514 Gomez-Heras, M., Benavente, D., Buergo, M.Á.D., Fort, R., 2004. Soluble salt minerals from pigeon
515 droppings as potential contributors to the decay of stone based Cultural Heritage. *European*
516 *Journal of Mineralogy* 16, 505–509. <https://doi.org/10.1127/0935-1221/2004/0016-0505>
517 Gunasekaran, S., Anbalagan, G., Pandi, S., 2006. Raman and infrared spectra of carbonates of calcite
518 structure. *Journal of Raman Spectroscopy* 37, 892–899. <https://doi.org/10.1002/jrs.1518>
519 Janssens, K., Van Grieken, R., 2004. *Non-destructive Micro Analysis of Cultural Heritage Materials*.
520 Elsevier.
521 Matović, V., Erić, S., Kremenović, A., Colomban, P., Srećković-Batočanin, D., Matović, N., 2012. The
522 origin of syngenite in black crusts on the limestone monument King's Gate (Belgrade
523 Fortress, Serbia) – the role of agriculture fertiliser. *Journal of Cultural Heritage* 13, 175–186.
524 <https://doi.org/10.1016/j.culher.2011.09.003>
525 Morillas, H., Maguregui, M., Paris, C., Bellot-Gurlet, L., Colomban, P., Madariaga, J.M., 2015. The role
526 of marine aerosol in the formation of (double) sulfate/nitrate salts in plasters. *Microchemical*
527 *Journal* 123, 148–157. <https://doi.org/10.1016/j.microc.2015.06.004>
528 Perdikouri, C., Piazzolo, S., Kasiotas, A., Schmidt, B.C., Putnis, A., 2013. Hydrothermal replacement of
529 Aragonite by Calcite: interplay between replacement, fracturing and growth. *European*
530 *Journal of Mineralogy* 25, 123–136. <https://doi.org/10.1127/0935-1221/2013/0025-2261>
531 Plummer, L.N., Wigley, T.M.L., 1976. The dissolution of calcite in CO₂-saturated solutions at 25°C and
532 1 atmosphere total pressure. *Geochimica et Cosmochimica Acta* 40, 191–202.
533 [https://doi.org/10.1016/0016-7037\(76\)90176-9](https://doi.org/10.1016/0016-7037(76)90176-9)
534 Reddy, M.M., Sherwood, S.I., Doe, B.R., 1986. Limestone and Marble Dissolution by Acid Rain: An
535 Onsite Weathering Experiment, in: *Materials Degradation Caused by Acid Rain*, ACS
536 Symposium Series. American Chemical Society, pp. 226–238. [https://doi.org/10.1021/bk-](https://doi.org/10.1021/bk-1986-0318.ch015)
537 [1986-0318.ch015](https://doi.org/10.1021/bk-1986-0318.ch015)
538 Rodriguez-Navarro, C., Doehne, E., Sebastian, E., 2000. How does sodium sulfate crystallize?
539 Implications for the decay and testing of building materials. *Cement and Concrete Research*
540 30, 1527–1534. [https://doi.org/10.1016/S0008-8846\(00\)00381-1](https://doi.org/10.1016/S0008-8846(00)00381-1)

541 Sabbioni, C., 2003. Mechanisms of air pollution damage to stone, in: *The Effects of Air Pollution on*
542 *the Built Environment*, Air Pollution Reviews. Imperial College Press, pp. 63–106.
543 https://doi.org/10.1142/9781848161283_0003

544 Sabbioni, C., Zappia, G., 1992. Atmospheric-derived element tracers on damaged stone. *Science of*
545 *The Total Environment* 126, 35–48. [https://doi.org/10.1016/0048-9697\(92\)90482-8](https://doi.org/10.1016/0048-9697(92)90482-8)

546 Saheb, M., Chabas, A., Mertz, J.-D., Colas, E., Rozenbaum, O., Sizun, J.-P., Nowak, S., Gentaz, L.,
547 Verney-Carron, A., 2016. Weathering of limestone after several decades in an urban
548 environment. *Corrosion Science* 111, 742–752. <https://doi.org/10.1016/j.corsci.2016.06.015>

549 Saheb, M., Mertz, J.-D., Colas, E., Rozenbaum, O., Chabas, A., Michelin, A., Verney-Carron, A., Sizun,
550 J.-P., 2014. Multiscale characterization of limestone used on monuments of cultural heritage,
551 in: *MRS Online Proceedings Library Archive*. Cambridge University Press, pp. 309–317.
552 <https://doi.org/10.1557/opl.2014.709>

553 Saheb, M., Verney-Carron, A., Remusat, L., Duhamel, R., Gonzalez-Cano, A., Mertz, J.-D., Loisel, C.,
554 Chabas, A., Rozenbaum, O., 2015. Isotope tracers to investigate reactive zones in stones from
555 built cultural heritage, in: *Procedia Earth and Planetary Science*. Presented at the 11th
556 Applied Isotope Geochemistry Conference (AIG-11), pp. 56–59.

557 Sessegolo, L., Verney-Carron, A., Saheb, M., Remusat, L., Gonzalez-Cano, A., Nuns, N., Mertz, J.-D.,
558 Loisel, C., Chabas, A., 2018. Long-term weathering rate of stained-glass windows using H and
559 O isotopes. *npj Mater Degrad* 2, 1–9. <https://doi.org/10.1038/s41529-018-0038-1>

560 Shahidzadeh-Bonn, N., Desarnaud, J., Bertrand, F., Chateau, X., Bonn, D., 2010. Damage in porous
561 media due to salt crystallization. *Phys. Rev. E* 81, 066110.
562 <https://doi.org/10.1103/PhysRevE.81.066110>

563 Smith, B.J., Viles, H.A., 2006. Rapid, catastrophic decay of building limestones: Thoughts on causes,
564 effects and consequences, in: *Heritage Weathering and Conservation*. Taylor and Francis,
565 London, pp. 191–197.

566 Thomen, A., Robert, F., Remusat, L., 2014. Determination of the nitrogen abundance in organic
567 materials by NanoSIMS quantitative imaging. *J. Anal. At. Spectrom.* 29, 512–519.
568 <https://doi.org/10.1039/C3JA50313E>

569 van der Lee, J., De Windt, L., 2002. *CHESSTutorial and Cookbook*. Updated Version for Version 3.0.
570 Ecole des Mines de Paris, Centre d'Information Géologique, Fontainebleau, France.

571 Visconti, F., Paz, J.M.D., Rubio, J.L., 2010. Calcite and gypsum solubility products in water-saturated
572 salt-affected soil samples at 25°C and at least up to 14 dS m⁻¹. *European Journal of Soil*
573 *Science* 61, 255–270. <https://doi.org/10.1111/j.1365-2389.2009.01214.x>

574

575 LIST OF FIGURES

576

577 Figure 1: Burst pulsed ToF-SIMS signal around 18 u; pulsed bursts (a), cumulative burst signal –
578 metasignal and a single pulse (b) and deconvolution using Gaussian peaks for the studied species (c).

579

580 Figure 2: Superposition of SEM secondary electron map and EDS map of Ca (in orange) and Si (in
581 blue) (a), of S (in purple) (b) and of K (in yellow) (c) for TA

582

583 Figure 3: Raman spectra for TA samples exposed 2 months (a) and 1 year (b) to enriched vapor and
584 reference Raman spectra for syngenite, calcite, niter and thenardite.

585

586 Figure 4: Superposition of ToF-SIMS and SEM secondary electron maps of D (red) and ^{18}O (yellow) for
587 TA sample exposed 2 months to enriched vapor.

588

589 Figure 5: Oxygen and hydrogen isotopic ratio obtained via ToF-SIMS at varying depth inside TA
590 sample exposed 2 months to enriched vapor and compared to reference naturally observed ratio.

591

592 Figure 6: TA sample exposed 2 months to enriched vapor: ToF-SIMS maps of a $150 \times 150 \mu\text{m}^2$ area for
593 ^{18}O (purple) and D (orange) and superposition of the ToF-SIMS D map with SEM-EDS map of sulfur S
594 (green).

595

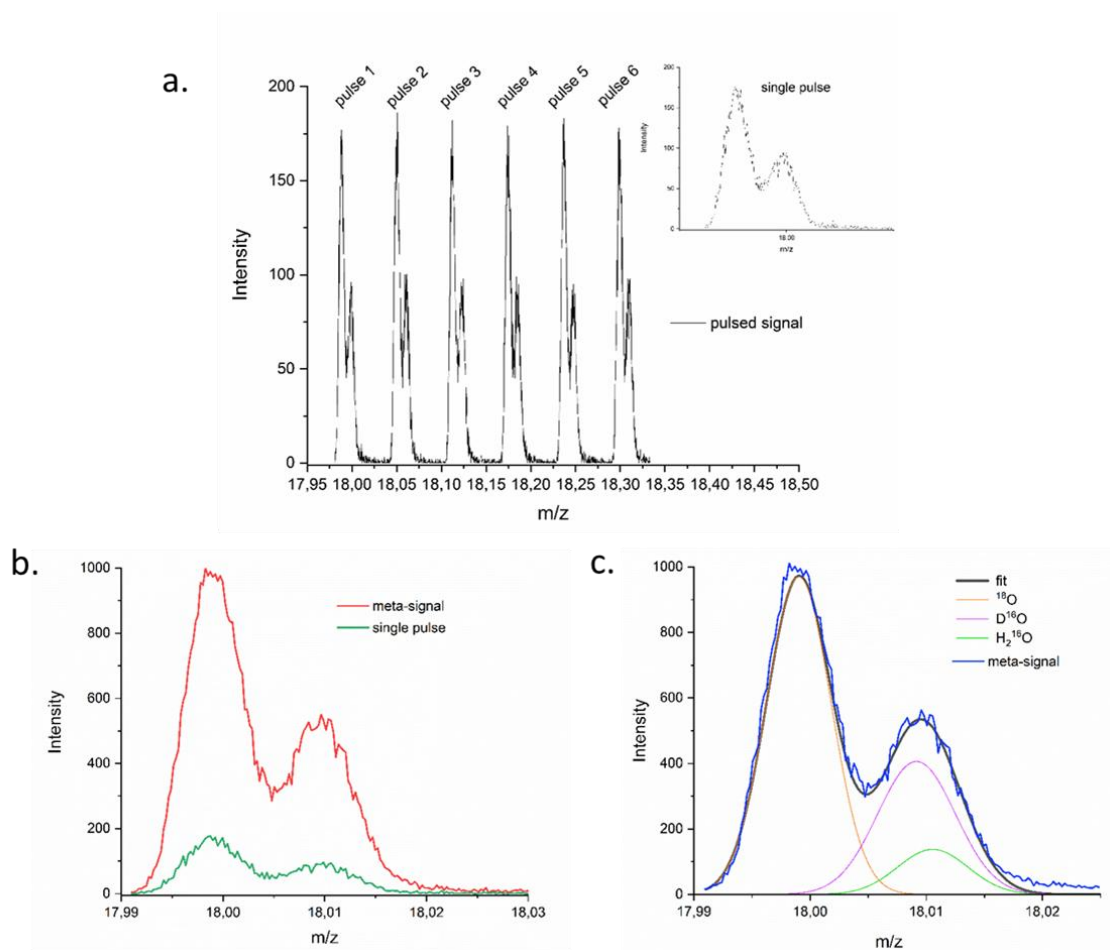
596 Figure 7: SEM (secondary electron) map (a) of the area of interest analyzed in NanoSIMS (white
597 square) and NanoSIMS maps of $f^{18}\text{O}$ (b) and fD (c), and of ^{12}C (d), ^{32}S (e) and ^{28}Si (f).

598

599

600

601 Figure 1.



602

603 Figure 1: Burst pulsed ToF-SIMS signal around 18 u; pulsed bursts (a), cumulative burst signal –

604 metasignal and a single pulse (b) and deconvolution using Gaussian peaks for the studied species (c).

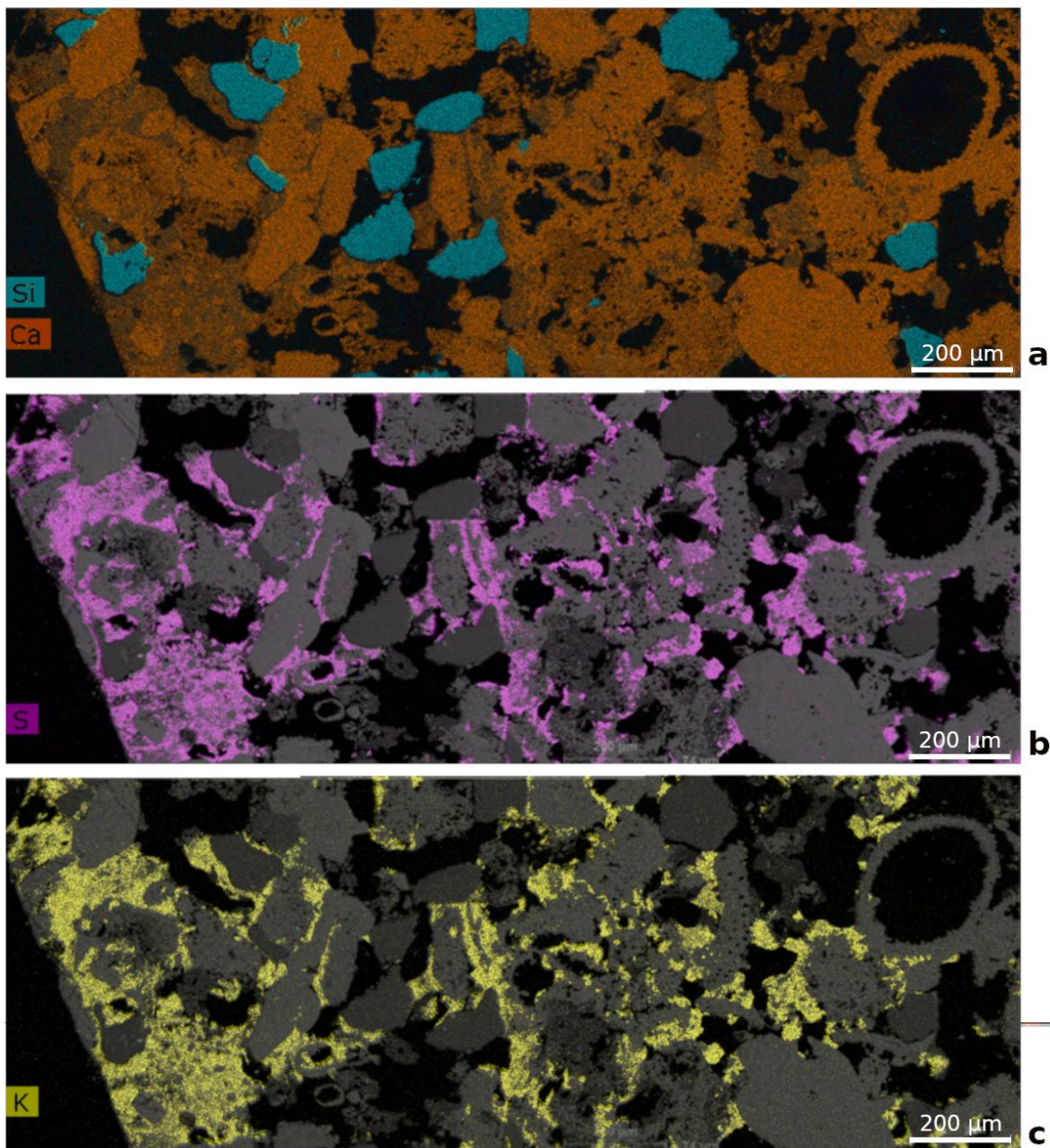
605

606

607

608 Figure 2.

609



610

611 Figure 2: Superposition of SEM secondary electron map and EDS map of Ca (in orange) and Si (in

612 blue) (a), of S (in purple) (b) and of K (in yellow) (c) for TA sample exposed 2 months to enriched

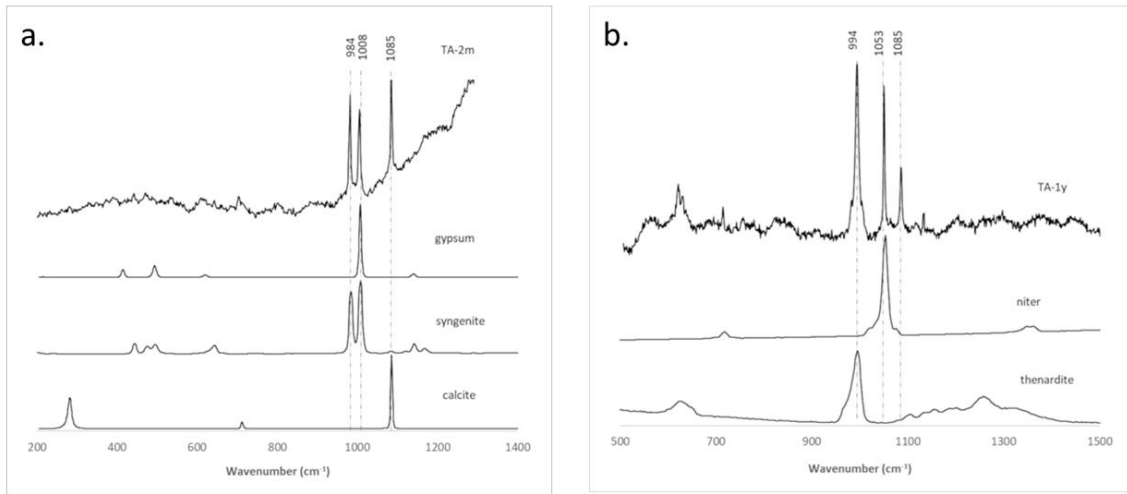
613 vapor.

614

615

616 Figure 3.

617



618

619 Figure 3: Raman spectra for TA samples exposed 2 months (a) and 1 year (b) to enriched vapor and

620

reference Raman spectra for syngenite, calcite, niter and thenardite.

621

622 Figure 4.

623



624

625 Figure 4: Superposition of ToF-SIMS and SEM secondary electron maps of D (red) and ¹⁸O (yellow) for

626

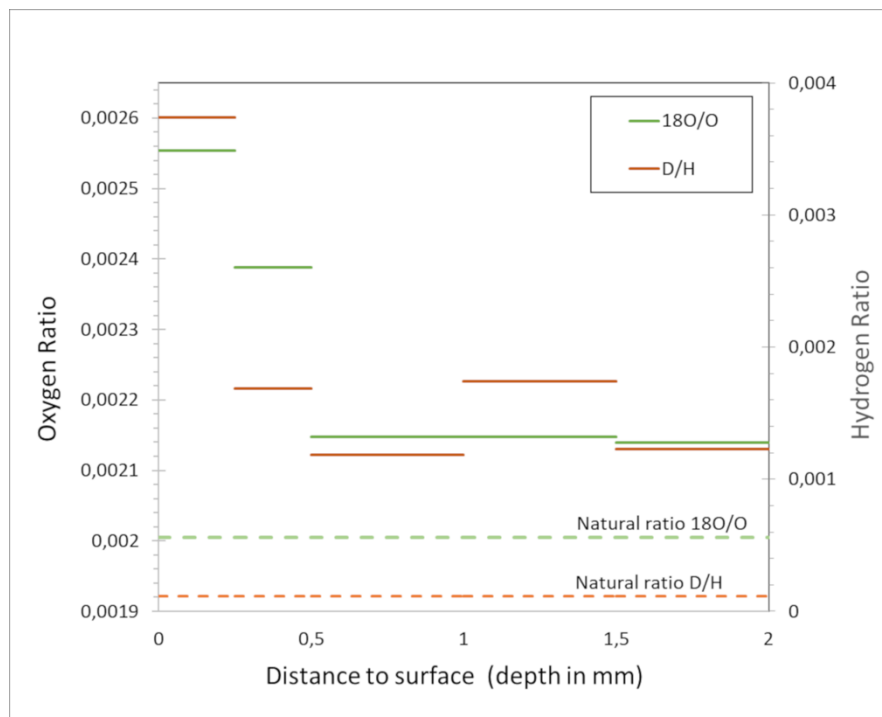
TA sample exposed 2 months to enriched vapor.

627

628

629 Figure 5.

630



631

632 Figure 5: Oxygen and hydrogen isotopic ratio obtained via ToF-SIMS at varying depth inside TA

633 sample exposed 2 months to enriched vapor and compared to reference naturally observed ratio.

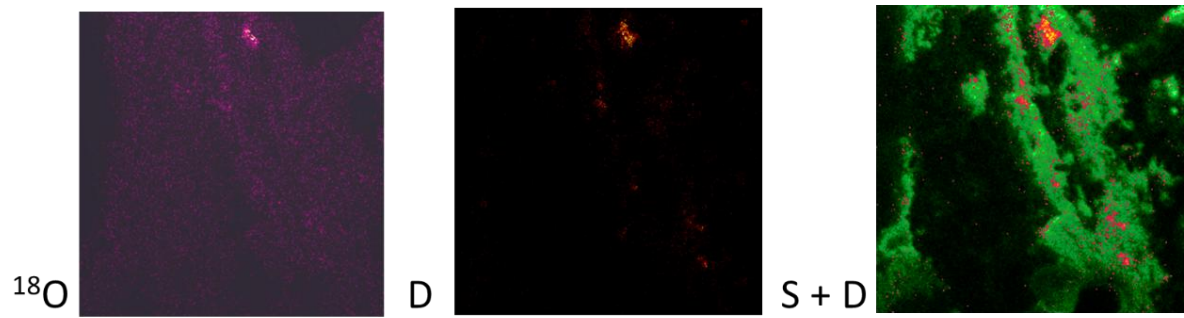
634

635

636

637 Figure 6.

638



639

640 Figure 6: TA sample exposed 2 months to enriched vapor: ToF-SIMS maps of a 150 x 150 μm^2 area for

641 ^{18}O (purple) and D (orange) and superposition of the ToF-SIMS D map with SEM-EDS map of sulfur S

642 (green).

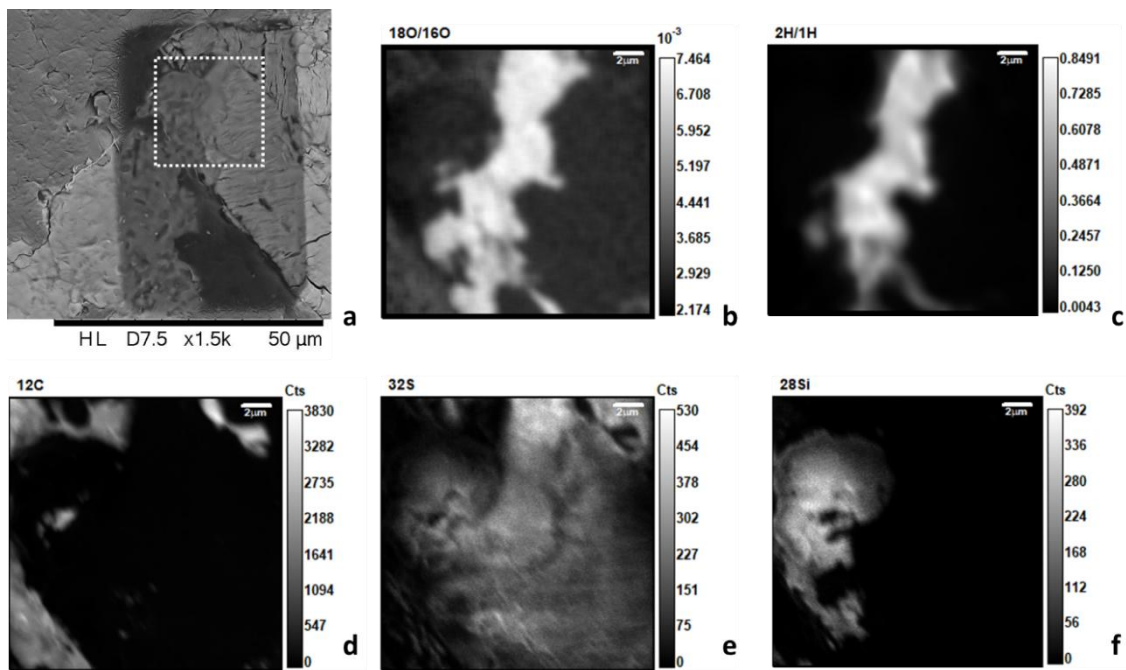
643

644

645

646 Figure 7.

647



648

649 Figure 7: SEM (secondary electron) map (a) of the area of interest analyzed in NanoSIMS (white

650

square) and NanoSIMS maps of $f^{18}\text{O}$ (b) and fD (c), and of ^{12}C (d), ^{32}S (e) and ^{28}Si (f).

651

652

653 Table 1: Isotopic fraction and enrichment factor compared to the natural abundance for D and ¹⁸O.

	Isotopic fraction (f)				Enrichment factor		
	Natural abundance	Experiment Solution	ToF-SIMS	NanoSIMS	Solution	ToF-SIMS	NanoSIMS
D	$1.15 \cdot 10^{-4}$	0.9	$1.19-3.74 \cdot 10^{-3}$	$2.64 \cdot 10^{-2}$	x 7800	x 10-30	x 230
¹⁸ O	$2.005 \cdot 10^{-3}$	0.1	$2.14-2.56 \cdot 10^{-3}$	$3.52 \cdot 10^{-3}$	x 50	x 1.07-1.27	x 1.75
D/ ¹⁸ O		9			156	9-24	7

654

655

656

Declaration of interests

The authors declare that they have no known competing financial interests or personal relationships that could have appeared to influence the work reported in this paper.

The authors declare the following financial interests/personal relationships which may be considered as potential competing interests: